IET Circuits, Devices & Systems

Research Article

IET Journals
The Institution of Engineering and Technology

1.8 V, 25.9 nW, 91.86 dB dynamic range second-order lowpass filter tunable in the range 4–100 Hz

ISSN 1751-858X
Received on 25th January 2019
Revised 20th June 2019
Accepted on 23rd June 2019
E-First on 24th October 2019
doi: 10.1049/iet-cds.2019.0031
www.ietdl.org

Jayaram Reddy Machha Krishna Reddy[1] ✉, *Tonse Laxminidhi*[1]

[1]*Department of Electronics and Communication Engineering, NITK Surathkal, Karnataka, India*

✉ *E-mail: jayaram.041@gmail.com*

Abstract: A second-order lowpass Butterworth filter with tunable bandwidth capable of offering a dynamic range of 91.86 dB operating on a supply voltage of 1.8 V is presented. The proposed filter is based on a sub-threshold source follower. The transistor bias currents are switched to enable the bandwidth tuning in the range 4–100 Hz. A proportional to absolute temperature (PTAT) current reference circuit helps to keep the bandwidth intact across process, voltage and temperature variations. The filter, designed in 0.18 µm standard CMOS process, consumes 25.9 nW making it a potential candidate for portable biomedical applications.

1 Introduction

Analog filters with low cut-off frequency are the essential building blocks in biomedical devices. The low-frequency lowpass filters (LPFs) are used to enhance the quality of sensed bio-signals by rejecting the out-of-band noise. The filters sense the bio-signals with frequencies <100 Hz and amplitude ranging from 1 µV to 100 mV [1]. The circuits processing these low amplitude bio-signals are required to exhibit sufficiently low input-referred noise (INR) and distortion to avoid input signal degradation.

The designed filters with low cut-off frequency are quite challenging for applications like portable and implantable biomedical devices. The filters are required to be ultra-low power to support small form-factor of batteries and to extend the battery back-up. In addition, they are also required to occupy as little area as possible for cost minimisations.

Switched capacitor (SC) filters are not suitable for low-frequency applications as they suffer from clock feed-through and leakage problems in advanced processes [2]. Active resistor-capacitor filters and passive resistor-inductor-capacitor filters are not preferred for biomedical applications, as large-sized components are needed to achieve low cut-off frequencies.

Transconductor–capacitor ($g_m - C$) filter topologies are widely used for low-frequency LPFs. In $g_m - C$ based topologies, the cut-off frequency is decided by the ratio g_m/C, where C is the integrating capacitance. Lower cut-off frequencies can be achieved by increasing C and/or decreasing g_m. However, capacitances used on-chip are limited to few tens of pico-farads because of silicon area limitations. With the small value of capacitance available on-chip, the minimum bandwidth that can be achieved is also limited. For fully on-chip solutions, impedance scaling techniques are used to increase the effective capacitance by utilising the Miller effect [3], but with increased complexity, power consumption, and noise.

Low bandwidth is also achieved by using transconductors of sufficiently low value. Several g_m reduction techniques are reported in the literature [3, 4], where the transconductor unit is modified to achieve a low value of g_m by techniques like multiple input floating gate, current division, source degeneration and bulk-driven. The detailed discussion on relative performance and limitations of these techniques has been presented in [5, 6].

In this paper, an alternative design for realising low-frequency LPFs has been presented. The design uses source-followers to realise the filter. The paper is organised as follows. In Section 2, sub-threshold source follower (SSF) biquad is illustrated. Second-order LPF based on the SSF biquad is presented in Section 3. Simulation results are presented in Section 4. Section 5 concludes the paper.

2 SSF-based biquadratic cell

A basic source follower circuit shown in Fig. 1 can be viewed as a first-order LPF, considering the capacitance at the output.

The transfer function is given by

$$H(s) = \frac{g_m r_{o,eq}}{sCr_{o,eq} + (g_m + g_{mb})r_{o,eq} + 1} \quad (1)$$

where g_m and g_{mb} are the gate transconductance and back-gate transconductance of the transistor M_1, respectively, $r_{o,eq}(= r_{o1} \parallel r_{o2})$ is the equivalent output resistance.

The source follower shown in Fig. 1 is extended to realise a bi-quadratic cell as shown in Fig. 2*a*. The circuit elements include four transistors ($M_1 - M_4$), four current sources ($I_b, 2I_b$) and two floating capacitors ($C_1/2, C_2/2$). Here, a positive feedback generated by transistors (M_2, M_3) is utilised to generate the complex conjugate poles required for the second-order response. Source follower based biquads are reported in [7]. However, the architecture shown in Fig. 2*a* has not been found to be explored further for low power, low frequency filter applications.

Source follower based biquads exhibit the following advantages: Additional common mode feedback circuit is not required as the output common mode voltage is self-biased by the transistor's, V_{GS}, saving area and power. The circuit is free from the effects of parasitics as only two nodes are present and they are the integrating nodes. Furthermore, there are no instability issues because of positive feedback as the loop gain is inherently <1. Also, it exhibits a low output impedance to drive the later stages

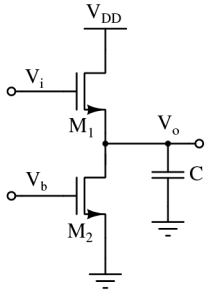

Fig. 1 *Basic source follower, with an output capacitor*

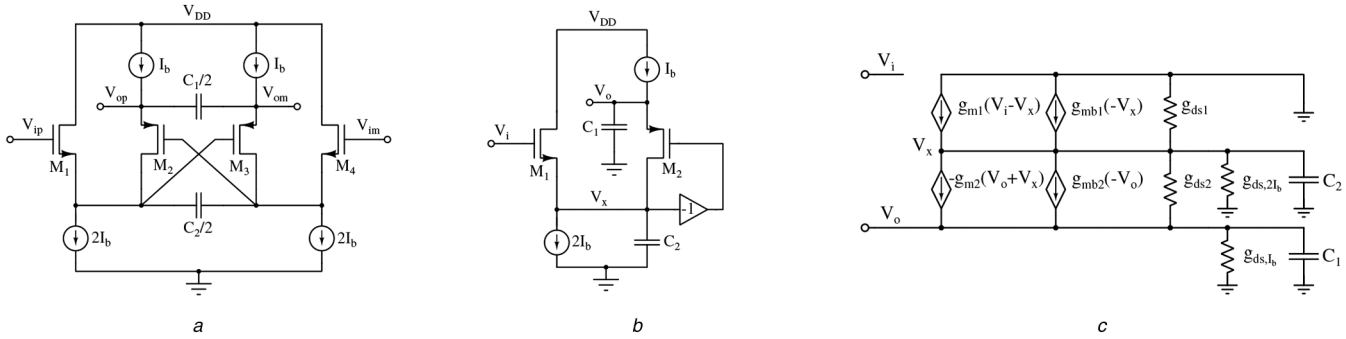

a *b* *c*

Fig. 2 *Source follower*
(a) Biquad, ***(b)*** Its equivalent half-circuit, ***(c)*** Small signal equivalent

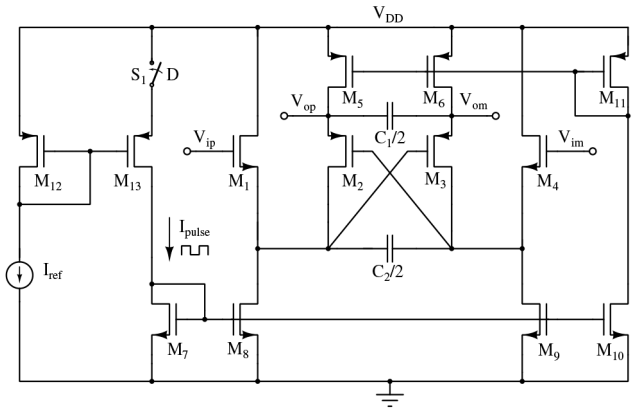

Fig. 3 *Schematic of switched second order LPF*

and offers excellent linearity, as the signal is processed in terms of voltage by local feedback. The equivalent half circuit of source follower biquad is as shown in Fig. 2*b*. It's small signal equivalent circuit is shown in Fig. 2*c*. The complete transfer function of the biquad is given by (2), where $g_{mn1} = g_{m1} + g_{mb1}$ and $g_{mp2} = g_{m2} + g_{mb2}$ (see (2)) . By neglecting body effect and channel length modulation, and if input transistors are designed to have equal gate transconductance g_m, the overall transfer function reduces to (3)

$$\frac{V_o}{V_i} = -\frac{1}{s^2\left(C_1C_2/g_m^2\right) + s(C_2/g_m) + 1} \tag{3}$$

The filter parameters (cut-off frequency ω_o and quality factor Q) are given by

$$\omega_o = \frac{g_m}{\sqrt{C_1C_2}} \tag{4}$$

$$Q = \sqrt{\left(\frac{C_1}{C_2}\right)} \tag{5}$$

Considering body effect, from (2) the passband gain A is expressed as,

$$A = \frac{g_m^2}{(g_m + g_{mb})^2} = \frac{1}{1 + (g_{mb}/g_m)^2} \tag{6}$$

where g_{mb}/g_m is the ratio of bulk transconductance to gate transconductance. The value of the ratio is in between 0.2 and 0.5 and therefore, the passband gain achievable is in the range −3.2 to −7.2 dB.

The cut-off frequency is decided by the ratio g_m/C. Practically, low cut-off frequencies are attained by reducing g_m. The value of g_m is reduced (to the order of nano-siemens) by operating the transistors in weak-inversion region. In weak-inversion region, g_m is given by $g_m = I_D/\eta V_T$, where η is the sub-threshold slope factor ($\simeq 1.0$), V_T is the thermal voltage ($\simeq$26 mV) and I_D is the drain current. Here, the g_m is reduced to nano-siemens by using a sufficiently low value of I_D, resulting in low power consumption.

3 Switched SSF biquad based second-order LPF

The bandwidth of the filter is further reduced by the technique of switched transconductor. Here, the filter cut-off is made tunable by switching the transconductors with a tunable duty ratio. This is achieved by switching bias currents of the transistors with a required duty-ratio (D). The schematic of switched second-order LPF based on source follower biquad cell is shown in Fig. 3.

3.1 Current reference with switching circuit

Small bias currents (of the order of nA) are more susceptible to variations in temperature. A slight variation in temperature can cause a large change in the current, resulting in a large deviation in g_m and hence the cut-off frequency. In weak-inversion region, $g_m = I_D/\eta V_T$. The thermal voltage V_T is proportional to the absolute temperature (PTAT) and therefore, g_m (and the cut-off frequency) decreases with the temperature. This can be easily mitigated with a PTAT drain current I_D. A classical beta multiplier circuit [8] has been modified suitably with cascode transistors and associated switching circuitry to generate a switched PTAT current reference required for the purpose. The complete current reference circuit is shown in Fig. 4*a*.

The sub-threshold current I_D through a PMOS transistor is given by

$$I_D = KI_{Do}\exp\left(\frac{V_{SG} - |V_{TH}|}{\eta V_T}\right)\left(1 - \exp\left(\frac{-V_{DS}}{\eta V_T}\right)\right) \tag{7}$$

where $K = W/L$ is the aspect ratio of transistor, $I_{Do} = \mu C_{ox}(\eta - 1)V_T^2$ is the pre-exponential factor of sub-threshold current, μ is the carrier mobility, C_{ox} is the gate-oxide capacitance and V_{TH} is the threshold voltage. For $V_{DS}4V_T$, (7) reduces to

$$I_D = KI_{Do}\exp\left(\frac{V_{SG} - |V_{TH}|}{\eta V_T}\right) \tag{8}$$

The reference current I_{ref} in Fig. 4*a* is expressed as

$$I_{ref} = \frac{V_{SG7} - V_{SG8}}{R} \tag{9}$$

$$\frac{V_o}{V_i} = -\frac{g_{m1}(g_{m2} - g_{ds2})}{(g_{mn1} - g_{m2} + g_{ds1} + g_{ds2} + g_{ds,2I_b} + sC_2)(g_{mp2} + g_{ds2} + g_{ds,I_b} + sC_1) + (g_{mp2} + g_{ds2})(g_{m2} - g_{ds2})} \tag{2}$$

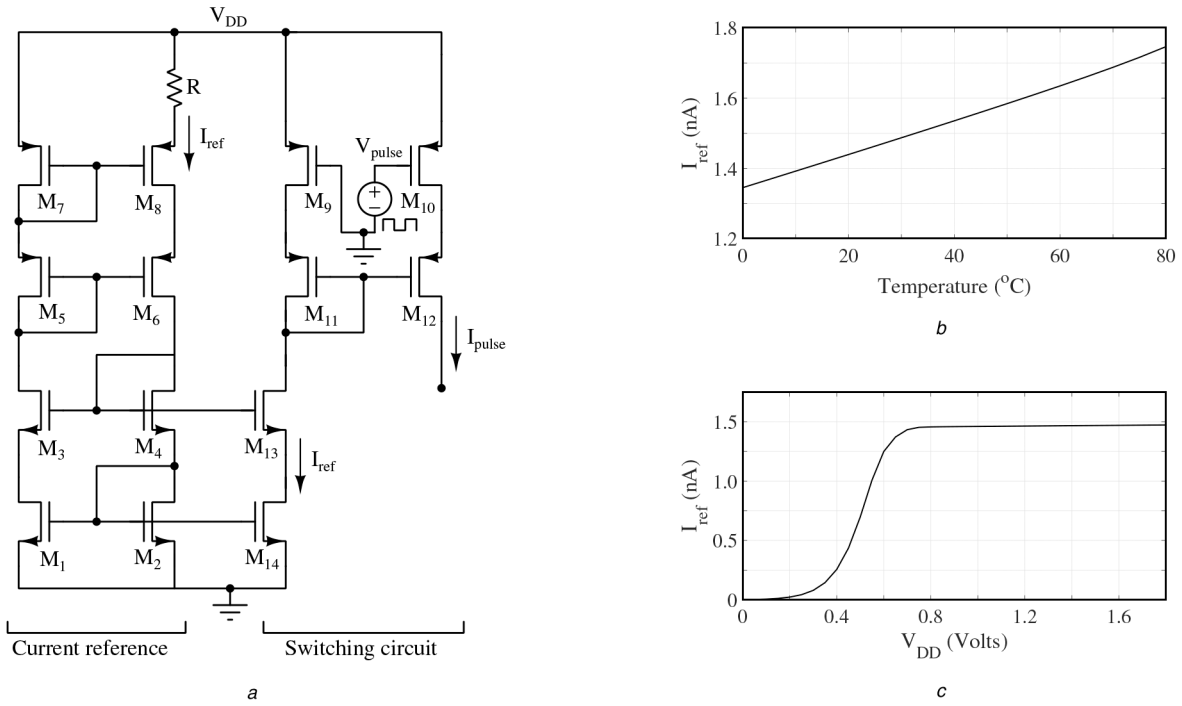

Fig. 4 *Current reference generator with switching*
(a) Complete schematic, ***(b)*** I_{ref} as a function of temperature, ***(c)*** I_{ref} as a function of V_{DD} at room temperature

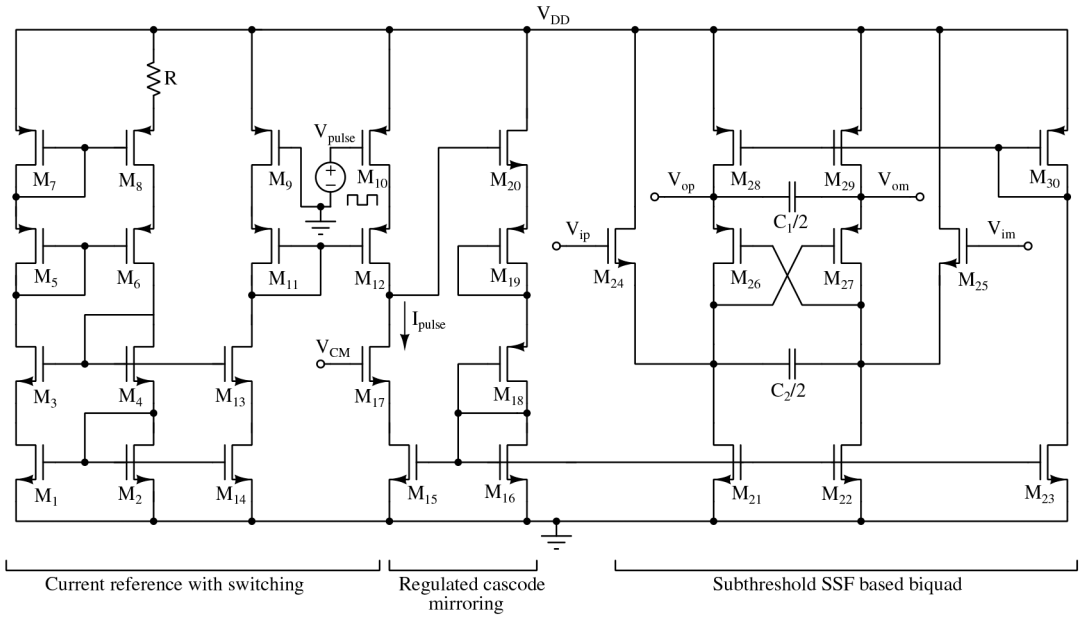

Fig. 5 *Complete schematic of the switched SSF biquad based second-order LPF*

Substituting for V_{SG7} and V_{SG8} from (8) and by considering same drain currents, I_{ref} is given by

$$I_{ref} = \frac{\eta V_T \ln(p)}{R} = \frac{\eta k T \ln(p)}{qR} \tag{10}$$

where $p = K_8/K_7 = (W/L)_8/(W/L)_7$ is the ratio of transistor sizes, k is the Boltzmann constant, T is the absolute temperature and q is the electron charge. With a thermally stable external resistor, the I_{ref} is found to be PTAT. In this work, $R = 10\,\text{M}\Omega$ is chosen to generate a nano-ampere current reference ($I_{ref} = 1.47\,\text{nA}$). From (10), it is also evident that the reference current varies proportional to the absolute temperature (PTAT) and it is clearly shown in Fig. 4*b*.

For the current reference circuit designed in this work, I_{ref} is plotted as a function of V_{DD} at room temperature in Fig. 4*c*. A line sensitivity of 0.9%/V is observed in a supply range of 0.8–1.8 V, proving that the reference current is almost independent of supply voltage. The generated current reference is mirrored and switched using the transistors $M_9 - M_{14}$ as shown in Fig. 4*a*. Here, the duty ratio of V_{pulse} is varied to switch the bias currents of the transconductors.

A complete schematic of the proposed switched SSF biquad based second-order LPF is as shown in Fig. 5. Regulated cascode current mirror has been used for accurate mirroring of the switched current. The transistor sizes for the proposed filter are listed in Table 1.

3.2 Noise analysis

The noise model of SSF biquad is shown in Fig. 6. In transistors, the major sources of noise are flicker noise and thermal noise. Flicker noise is dominated at lower frequencies and thermal noise at higher frequencies. For noise analysis, both flicker noise and

Table 1 Transistor sizes of the proposed filter

Transistor	W, μm/L, μm
$M_{1-4,13,14}$	2 (2/1)
$M_{5,7}$	2 (6/1)
$M_{6,8}$	2 (9/1)
M_{9-12}	2 (1/0.5)
M_{15}	4 (12/18)
M_{16}	6 (16/18)
M_{17}	6 (16/18)
M_{18-20}	2 (1/10)
$M_{21,22,24,25}$	4 (12/18)
M_{23}	4 (6/18)
M_{26-30}	6 (16/12)

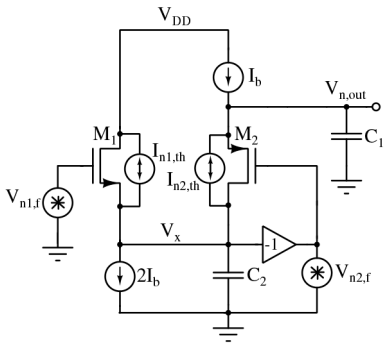

Fig. 6 *Equivalent noise model for analysis*

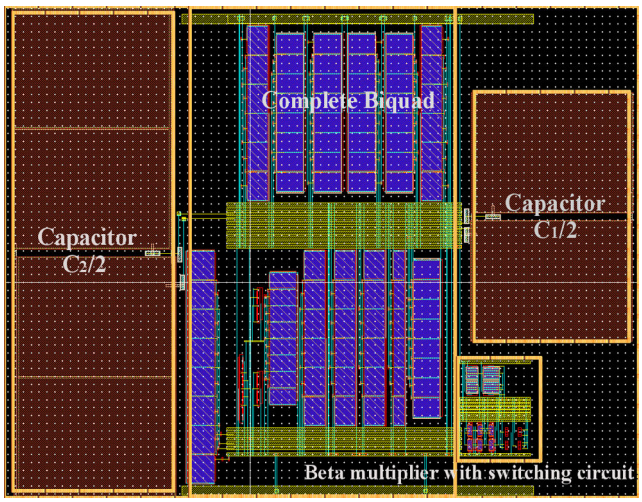

Fig. 7 *Complete layout of the switched SSF biquad filter*

Table 2 Summary of the filter performance at 1.8 V supply

Parameters	Values
total current, nA	14.42
power, nW	25.95
DC gain, dB	−3.25
filter order	2
bandwidth, Hz	4–100
linearity @1% THD ($V_{\text{in,pk-pk}}$ (mV) @ 10 Hz)	996
IRN (μV_{rms}) (100 mHz–100 Hz)	8.985
dynamic range, dB	91.86

thermal noise are considered. The IRN of the biquad integrated over the passband is given by

$$\overline{V_{\text{n,in}}^2} = \left(\overline{V_{\text{n,in,th}}^2} + \overline{V_{\text{n,in,f}}^2}\right) \cdot \Delta f \tag{11}$$

$$\overline{V_{\text{n,in}}^2} = \frac{4kT\gamma}{g_{\text{m1}}}\left[1 + \frac{g_{\text{mn1}}^2}{g_{\text{m1}}g_{\text{m2}}}\right] \cdot \Delta f + \frac{K_{\text{F}}}{C_{\text{ox}} \cdot f}\left[\frac{1}{(WL)_1} + \frac{g_{\text{mn1}}^2}{(WL)_2 \cdot g_{\text{m1}}^2}\right] \cdot \Delta f \tag{12}$$

where, γ is the noise co-efficient, K_{F} is the flicker noise coefficient and f is the frequency. Flicker noise, being inversely proportional to the transistor gate area, is reduced by choosing a large sized transistor. By reducing the flicker noise, thermal noise is made the dominant contributor. The thermal noise integrated over the passband is given by

$$\overline{V_{\text{n,in}}^2} = \frac{4kT\gamma}{\sqrt{C_1C_2}}\sqrt{\frac{g_{\text{m2}}}{g_{\text{m1}}}}\left[1 + \frac{g_{\text{mn1}}^2}{g_{\text{m1}}g_{\text{m2}}}\right] \tag{13}$$

Assuming that all transistors have same gate transconductanes and by neglecting body-effect, the thermal noise is equal to

$$\overline{V_{\text{n,in}}^2} = \frac{8kT\gamma}{\sqrt{C_1C_2}} \tag{14}$$

From (14), it is evident that thermal noise reduces with higher load capacitors. In the proposed filter, with the value of capacitors used the noise offered is less.

4 Simulation results

The proposed switched SSF biquad based Butterworth second-order LPF is designed using UMC 0.18 µm CMOS technology. The filter is designed to operate in the weak inversion region with a supply voltage of 1.8 V. The complete layout of the filter is shown in Fig. 7. The layout area is 0.121 mm^2. Post layout simulations are carried out to evaluate the filter performance. The summary of the filter performance is shown in Table 2.

The magnitude response of the filter for varying duty ratio (D) of the current pulse is shown in Fig. 8*a*. The filter cut-off frequency f_{c} is tunable from 4 to 100 Hz for 1–100% duty ratio of the current pulse. Note that, the clock frequency is modified suitably to keep clock feed-through out of stop-band frequency (corresponding to attenuation of 100 dB). The integrating capacitors for the filter are $C_1/2 = 15.25$ pF and $C_2/2 = 30.50$ pF including parasitics, for the transconductance of 27.23 nS ($g_{\text{m}} \simeq g_{\text{m1}} \simeq g_{\text{m2}}$) to achieve bandwidth of 100 Hz with 100% duty ratio. Fig. 8*b* shows the cut-off frequency of the filter as a function of duty ratio. It is evident that cut-off frequency varies linearly with duty ratio except at 4 Hz. Clock feed-through charge on capacitor starts dominating over that from the switched transconductor (due to low on-time) and capacitor charge/discharge due to junction leakage (due to large off time). Monte-Carlo simulation has been carried out on the layout extracted filter to evaluate the performance in the presence of transistor mismatches. Fig. 8*c* shows the distribution of filter cut-off frequency for 200 samples for $f_{\text{c}} = 100$ Hz (with $D = 100\%$). A mean of 100.1 Hz and standard deviation (σ) of 4.62 Hz are obtained. The sizes are chosen sufficiently large to keep the INR at a sufficiently low value. This in turn helps to keep the mismatch and hence the input offset to a low value [9].

Post layout simulations are carried out across process corners, supply voltage and temperature (PVT) variations, for a setting of $f_{\text{c}} = 100$ Hz. Fig. 9*a* shows the frequency response of the filter at various process corners. The change in cut-off frequency f_{c} is <1% at nominal supply voltage of 1.8 V and at room temperature (27°C).Fig. 9*b* shows the magnitude response for ±10% variation in supply voltage from the nominal value at typical process corner and room temperature. The change in bandwidth is <5%. For a temperature in the range 0–80°C at nominal supply voltage and typical corner, the bandwidth variation is <5% as shown in Fig. 9*c*. It is to be noted that the robustness of bandwidth against temperature is due to the PTAT current reference circuit. This is evident from Fig. 9*d* where it can be clearly seen that the filter

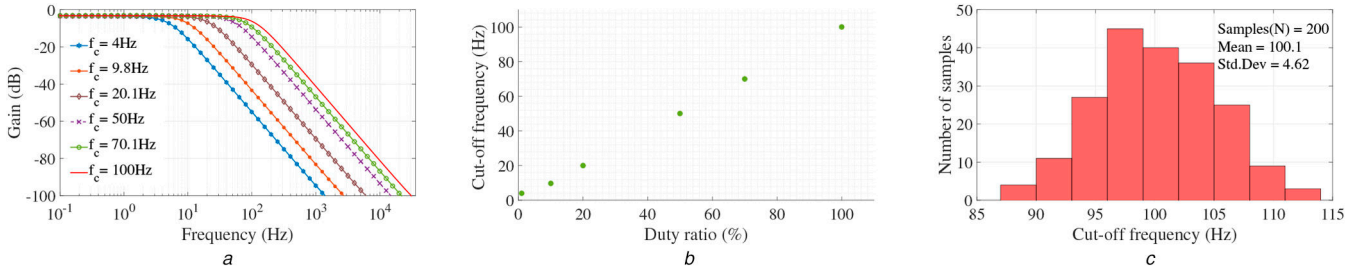

Fig. 8 *Filter response*

(a) Magnitude response of the filter with duty ratio tuning. The tuning range is from 4 to 100 Hz. The following settings are used for the results and in the format [clock frequency, duty cycle, cut-off frequency]: [1 kHz, 1%, 4 Hz], [10 kHz, 10%, 9.8 Hz], [10 kHz, 20%, 20.1 Hz], [20 kHz, 50%, 50 Hz], [20 kHz, 70%, 70.1 Hz], [20 kHz, 100%, 100 Hz], ***(b)*** Tuning graph showing f_c for different values of duty ratio, ***(c)*** Monte-Carlo simulation of the filter with 200 runs for $f_c = 100$ Hz setting

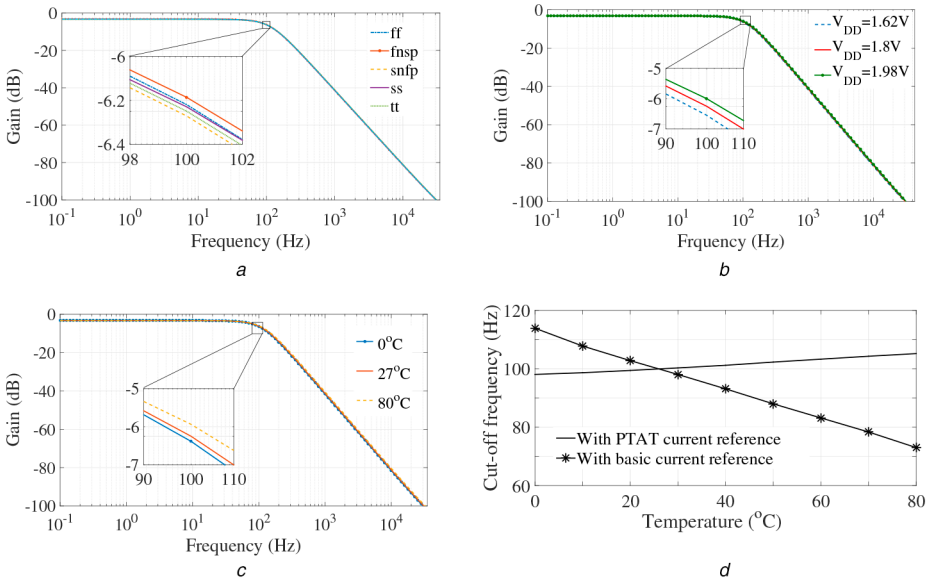

Fig. 9 *Magnitude response*

(a) Across process corner variations, ***(b)*** Across supply variations, and ***(c)*** Across temperature variations, ***(d)*** Cut-off frequency (f_c) vs. temperature (T)

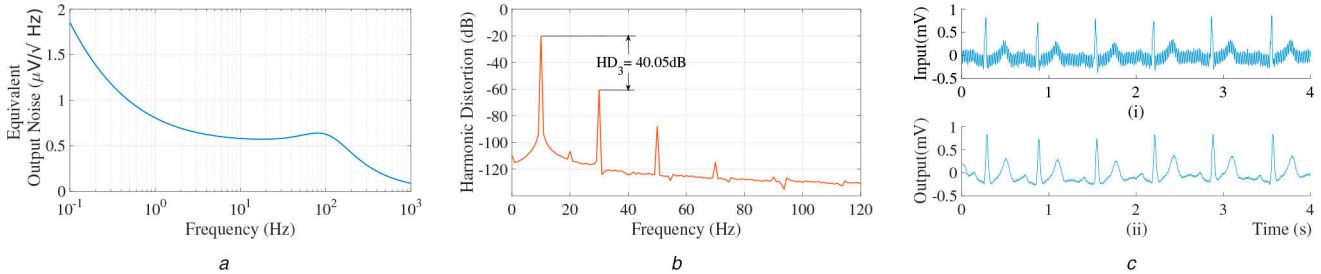

Fig. 10 *Filter Performance*

(a) Output-referred noise of the filter, ***(b)*** Harmonic distortion of the filter with $V_{in} = 996\,mV_{pp}$ @ 10 Hz, ***(c)*** The post layout filter test for ECG:(i). The time representation of the original ECG signal (ii). The filtered ECG signal obtained from the proposed LPF (Normalised for DC gain)

exhibits a poor bandwidth stability with temperature when a constant current reference is used.

These deviations can be tuned back by re-adjusting D appropriately.

The output referred noise of the filter is shown in Fig. 10*a*. The overall noise contributed by the filter is well within the permissible range. For biomedical applications, the acceptable in-band INR of the filter is given by (as in [10, 11])

$$\text{Noise}_{\text{in,ref}}(\text{rms}) \leq \frac{V_{\text{in,rms}}}{10^{\text{SNR(dB)}/20}} \tag{15}$$

where $V_{\text{in,rms}}$ is the given input voltage and SNR is signal-to-noise ratio of the filter. From [10], for filtering biomedical signals like ECG, the SNR requirement of the filter is ≥38 dB. Similarly, for EEG the requirement on SNR is ≥40 dB [12]. With the dynamic range offered in excess of 90 dB, the overall noise contributed by proposed filter is well within the acceptable range to cause any notable performance degradation. The proposed filter can process input voltage up to 996 mV_{pp}. As per (15), for SNR > 40 dB the in-band INR of the filter must be <3.52 mV_{rms}. Therefore, the proposed filter offering INR of 8.985 μV_{rms} is indeed the best candidate for filtering bio-signals.

The linearity performance of the filter is evaluated by single tone test, for an input voltage of 996 mV_{pp} at 10 Hz. Fig. 10*b* shows output voltage spectrum of the filter. Even-order harmonics are inherently rejected due to fully differential architecture of the filter. Third harmonic component is the dominant contributor and third harmonic distortion (HD3) is found to be −40.05 dB. HD3 is associated with a 1% THD (total harmonic distortion) as higher order harmonics are negligible. An un-filtered original ECG signal shown in Fig. 10*c*(i) obtained from [13] is provided as an input to the proposed LPF with 10 Hz bandwidth. The output of the LPF is

Table 3 Comparison of the filter performance with prior works found in the literature

Parameters	Supply voltage, V	Technology,μm	Power, μW	DC gain, dB	Filter order	Bandwidth f_c, Hz	THD, dB	IRN, μV_{rms}	DR	FoM, J
[14] [2013]	3	0.35	0.015	0	4	100	−60.7	29	64.8	2.15×10^{-14}
[15] [2014]	3	0.35	6.31	—	2	1.95	−40	791	50.65	4.74×10^{-9}
[16] [2015]	1.5	0.35	0.0019	0	2	250	−40	89	59.6	3.97×10^{-15}
[17] [2016]	0.9	0.13	0.8	4.1	2	47.98	−40	17.38	43.8	5.38×10^{-11}
[18] [2018]	1.8	0.18	2.7	0	1	5	−40	12.8	>80	5.40×10^{-11}
[19] [2018]	0.9	0.35	0.00426	−0.05	4	100	−40	80.5	48.2	4.14×10^{-14}
[20] [2018]	1	0.18	0.35	−8	5	50	−49.9	97	49.8	4.53×10^{-12}
[21] [2018]	1.5	0.35	0.0052	0.06	4	99	−40	43.9	59.7	1.35×10^{-14}
[22] [2018]	1	0.18	1.75	0	1	1	−40	11.3	>70	5.53×10^{-10}
[23] [2018]	1.8	0.18	0.689	21.8[a]	3[a]	200	—	81.79	—	—
[24] [2018]	0.6	0.35	0.009	−2.77	4	101	−41	46.27	47	9.95×10^{-14}
[25] [2018]	1	0.18	0.041	−7	5	250	—	134	61.2	2.85×10^{-14}
[26] [2018]	1.5	0.35	0.00525	−0.09	4	100	−40	39.38	56.9	1.87×10^{-14}
this work	1.8	0.18	0.0259	−3.25	2	100	−40	8.985	91.86	3.30×10^{-15}

[a]With pre-amplifier.

as shown in Fig. 10*c*(ii), and it is clearly seen that the filter is successful in extracting the signal from the noise.

Table 3 compares the filter performance with the state-of-the-art filters. To validate the results, the switching duty-ratio is set to 100% with $I_b = 1.47$ nA ($f_c = 100$ Hz setting). The filter with a high dynamic range (DR) of 91.86 dB is the best when compared to other filters found in the literature. To compare the performance of the proposed filter with other filters, figure-of-merit (FoM) [26, 27] is used

$$\text{FoM} = \frac{\text{Power}}{\text{Order} \times f_c \times \text{Dynamic range}} \tag{16}$$

It can be clearly seen that, with its energy efficiency (FoM), the proposed filter stands as one of the best candidates for biomedical signal processing.

5 Conclusion

A low-power, second-order, switched sub-threshold source follower biquad based filter has been presented. Switching technique used for the filter allowed the cut-off frequency to be adjusted from 4 to 100 Hz. The filter is found to offer a very good linearity and noise performance when compared to the widely used $g_m - C$ topology. Also, power efficiency and FoM is found to be on-par with the state-of-the-art filter found in the literature. As the overall power consumed by the filter is only 25.95 nW, the proposed filter is best suited for portable and implantable biomedical devices.

6 Acknowledgment

The authors would like to thank Ministry of Electronics and Information Technology (MeitY), Government of India, for providing the EDA tools support through SMDP-C2SD project.

7 References

[1] Harrison, R.R.: 'A versatile integrated circuit for the acquisition of biopotentials'. Proc. IEEE 2007 Custom Integrated Circuits Conf. (CICC), San Jose, CA, USA, 2007, pp. 115–122

[2] Nagaraj, K.: 'A parasitic-insensitive area-efficient approach to realizing very large time constants in switched-capacitor circuits', *IEEE Trans. Circuits Syst.*, 1989, **36**, (9), pp. 1210–1216

[3] Sols Bustos, S., Silva Martnez, J., Maloberti, F., *et al.*: 'A 60-dB dynamic-range CMOS sixth-order 2.4-Hz low-pass filter for medical applications', *IEEE Trans. Circuits Syst. II, Analog Digit. Signal Process.*, 2000, **47**, (12), pp. 1391–1398

[4] Veeravalli, A., Sánchez Sinencio, E., Silva Martnez, J.: 'Transconductance amplifier structures with very small transconductances: a comparative design approach', *IEEE Trans. Solid-State Circuits*, 2002, **37**, (6), pp. 770–775

[5] Zhou, L., Chakrabartty, S.: 'Design of low-gm transconductors using varactor-based degeneration and linearization technique'. 2015 IEEE Biomedical Circuits and Systems Conf. (BioCAS), Atlanta, GA, USA, 2015, pp. 1–4

[6] Jayaram Reddy, M.K, Polineni, S., Laxminidhi, T.: '91 dB dynamic range 9.5 nW low pass filter for bio-medical applications'. Proc. 2018 IEEE Computer Society Annual Symp. on VLSI (ISVLSI), Hong Kong, China, 2018, pp. 453–457

[7] D'Amico, S., Conta, M., Baschirotto, A.: 'A 4.1-mW 10-MHz fourth-order source-follower-based continuous-time filter with 79-dB DR', *IEEE J. Solid-State Circuits*, 2006, **41**, (12), pp. 2713–2719

[8] Vittoz, E., Fellrath, J.: 'CMOS analog integrated circuits based on weak inversion operation', *IEEE J. Solid-State Circuits*, 1977, **12**, (3), pp. 224–231

[9] Akbari, M., Hashemipour, O., Moradi, F.: 'Input offset estimation of CMOS integrated circuits in weak inversion', *IEEE Trans. Very Large Scale Integr. (VLSI) Syst.*, 2018, **26**, (9), pp. 1812–1816

[10] Lee, S.Y., Cheng, C.J.: 'Systematic design and modeling of a OTA-C filter for portable ECG detection', *IEEE Trans. Biomed. Circuits Syst.*, 2009, **3**, (1), pp. 53–64

[11] Jayaram Reddy, M.K., Laxminidhi, T.: 'Widely tunable low pass gm-C filter for bio-medical applications', *IET Circuits Devices Syst.*, 2018, **13**, (2), pp. 239–244

[12] Bronzino, J.D.: '*Medical devices and systems*' (CRC Press, Boca Raton, Florida, USA, 2006)

[13] PHYSIONET: 'ECG-ID Database', 2018. Available http://wwwphysionetorg/cgi-bin/atm/ATM

[14] Zhang, T.T., Mak, P.I., Vai, M.I., *et al.*: '15-nW biopotential LPFs in 0.35 μm CMOS using subthreshold-source-follower biquads with and without gain compensation', *IEEE Trans. Biomed. Circuits Syst.*, 2013, **7**, (5), pp. 690–702

[15] Doménech Asensi, G., Carrillo Calleja, J.M., Illade Quinteiro, J., *et al.*: 'Low-frequency CMOS bandpass filter for PIR sensors in wireless sensor nodes', *IEEE Sens. J.*, 2014, **14**, (11), pp. 4085–4094

[16] Sawigun, C., Pawarangkoon, P.: 'A compact subthreshold CMOS 2nd-order gm-C lowpass filter'. Proc. 12th Int. Conf. on Electrical Engineering Electronics, Computer, Telecommunications and Information Technology (ECTI-CON), Hua Hin, Thailand, 2015, pp. 1–4

[17] Arya, R., Oliveira, J.P.: 'Gm-C biquad filter for low signal sensor applications'. Proc. 2016 MIXDES - 23rd Int. Conf. Mixed Design of Integrated Circuits and Systems, Lodz, Poland, 2016, pp. 207–210

[18] Pérez Bailón, J., Márquez, A., Calvo, B., *et al.*: 'A 0.18 μm CMOS widely tunable low pass filter with sub-Hz cutoff frequencies'. Proc. 2018 IEEE Int. Symp. on Circuits and Systems (ISCAS), Florence, Italy, 2018, pp. 1–4

[19] Thanapitak, S., Sawigun, C.: 'A subthreshold buffer-based biquadratic cell and its application to biopotential filter design', *IEEE Trans. Circuits Syst. I, Regul.Pap.*, 2018, **65**, (9), pp. 2774–2783

[20] Sun, C.Y., Lee, S.Y.: 'A fifth-order butterworth OTA-C LPF with multiple-output differential-input OTA for ECG applications', *IEEE Trans. Circuits Syst. II, Express Briefs*, 2018, **65**, (4), pp. 421–425

[21] Thanapithak, S., Sawigun, C.: 'A 1.5 V 5.2 nW 60 dB-DR lowpass filter with self-compansated gain in 0.35 μm CMOS suitable for biomedical applications'. Proc. 2018 IEEE Int. Symp. on Circuits and Systems (ISCAS), Florence, Italy, 2018, pp. 1–4

[22] Pérez Bailón, J., Márquez, A., Calvo, B., *et al.*: 'A 1 V–1.75 μW Gm-C low pass filter for bio-sensing applications'. Proc. 2018 IEEE 9th Latin American Symp. on Circuits & Systems (LASCAS), Puerto Vallarta, Mexico, 2018, pp. 1–4

[23] Deo, A., Pandey, S.K., Joshi, A., *et al.*: 'Design of a third order butterworth Gm-C filter for EEG signal detection application'. Proc. 2018 25th Int. Conf. 'Mixed Design of Integrated Circuits and System'(MIXDES), Gdynia, Poland, 2018, pp. 361–365

[24] Sawigun, C., Thanapitak, S.: 'A 0.9-nW, 101-Hz, and 46.3-μVrms IRN lowpass filter for ECG acquisition using FVF biquads', *IEEE Trans. Very Large Scale Integr. (VLSI) Syst.*, 2018, **26**, (11), pp. 2290–2298
[25] Lee, S.Y., Wang, C.P., Chu, Y.S.: 'Low-voltage OTA-C filter with an area-and power-efficient OTA for biosignal sensor applications', *IEEE Trans. Biomed. Circuits Syst.*, 2018, **13**, (1), pp. 56–67
[26] Sawigun, C., Thanapitak, S.: 'A nanopower biopotential lowpass filter using subthreshold current-reuse biquads with bulk effect self-neutralization', *IEEE Trans. Circuits Syst. I, Regul.Pap.*, 2018, **66**, (5), pp. 1746–1757
[27] Vittoz, E.A., Tsividis, Y.P.: 'Frequency-dynamic range-power', in Toumazou, C., Moschytz, G.S., Gilbert, B. (Eds.): '*Trade-offs in analog circuit design*' (Springer, Boston, Massachusetts, 2002), pp. 283–313